J. Ocean Univ. China (Oceanic and Coastal Sea Research)
https://doi.org/10.1007/s11802-021-4540-7
ISSN 1672-5182, 2021 20 (5): 1027-1036
http://www.ouc.edu.cn/xbywb/
E-mail:xbywb@ouc.edu.cn

Precipitation Distribution of the Extended Global Spring–Autumn Monsoon and Its Possible Formation Mechanism

QIN Ling[1), 2)], HUANG Fei[1), 2), 3)], and XU Shibin[1), 2), *]

1) *Key Laboratory of Physical Oceanography*, *Ocean University of China*, *Qingdao* 266100, *China*
2) *Laboratory for Ocean and Climate Dynamics*, *Pilot National Laboratory for Marine Science and Technology (Qingdao)*, *Qingdao* 266100, *China*
3) *Ningbo Collaborative Innovation Center of Nonlinear Hazard System of Ocean and Atmosphere*, *Ningbo University*, *Ningbo* 315211, *China*

(Received March 23, 2020; revised July 27, 2020; accepted January 4, 2021)

Abstract The global monsoon (GM) comprises two major modes, namely, the solstitial mode and equinoctial asymmetric mode. In this paper, we extend the GM domain from the tropics to the global region and name it the global spring – autumn monsoon (GSAM), which mainly indicates a spring–autumn asymmetrical precipitation pattern exhibiting annual variation. Its distribution and possible formation mechanisms are also analyzed. The GSAM domain is mainly distributed over oceans, located both in the midlatitude and tropical regions of the Pacific and Atlantic. In the GSAM domains of both the Northern and Southern Hemispheres, more precipitation occurs in local autumn than in local spring. The formation mechanisms of GSAM precipitation vary according to the different domains. GSAM precipitation in the tropical domain of the Eastern Hemisphere is influenced by the circulation differences between the onset and retreat periods of the Asian summer monsoon, while tropical cyclone activities cause precipitation over the South China Sea (SCS) and western North Pacific (WNP). GSAM precipitation in the tropical domain of the Western Hemisphere is influenced by the tropical asymmetrical circulation between the Northern and Southern Hemispheres and the variation in the intertropical convergence zone (ITCZ) driven by the intensity of the sea surface temperature cold tongues over the equatorial eastern Pacific and eastern Atlantic. GSAM precipitation in the midlatitude domain is influenced by the differences in water vapor transportation and convergence between spring and autumn. In addition, GSAM precipitation is also affected by extratropical cyclone activities.

Key words global monsoon; equinoctial asymmetric mode; monsoon precipitation; mechanism

1 Introduction

The global monsoon (GM) region is defined as the area where precipitation exhibits a reversal behavior between two seasons in an annual cycle (Wang, 1994a), and it is the most influential part of human activities. Monsoon precipitation plays a very important role in the global water cycle and in the relationship between the radiative equilibrium and atmospheric circulation (Chao, 2000; Gadgil, 2003). The influencing factors of GM precipitation are complex (Kim *et al.*, 2008; Zhou *et al.*, 2008; Liu *et al.*, 2009; Wang *et al.*, 2012); thus, it is essential to improve understanding of the variations in monsoon precipitation and its mechanisms.

Wang and Ding (2008) defined GM as the dominant mode of annual variation in global tropical circulation. They identified two major GM modes, namely, the solstitial mode and equinoctial asymmetric mode. The GM equinoctial asymmetric mode accounts for 13% of the total variance and exhibits precipitation asymmetry between spring and autumn, which mostly occurs in the tropical oceans of both the southern and northern hemispheres. Bombardi *et al.* (2019) provided another similar result. Analyzing the monsoon onset and retreat date, two wet seasons are identified. The first wet season onsets in the local summer and retreats in the local winter, while the second wet season onsets in the local autumn and retreats in the local spring. The precipitation distribution patterns from the result of Bombardi's study are similar to the precipitation patterns in Wang and Ding's research (2008).

The possible causes of this precipitation asymmetry have been studied in different regions (Chang *et al.*, 2005). In the Eastern Hemisphere, the precipitation reversal between spring and autumn occurs mainly in the South Asian maritime continental region and may be caused by the wind-terrain interactions and low-level divergence induced by the different land-ocean thermal inertia effects in the region. In addition, the precipitation patterns in South- east China from early summer to late summer (May–August) are studied (Liu *et al.*, 2020), and the precipitation patterns show different signals in early Meiyu season, and late

* Corresponding author. E-mail: xushibin@ouc.edu.cn

summer. During early summer (May–mid-June), the precipitation pattern in Southeast China mainly represents a dipole mode between coastal southeastern China and the Yangtze River Basin, which is only related to midlatitude wave trains due to the weak western North Pacific (WNP) monsoon trough during this period. Meanwhile, during the Meiyu season (mid-June–mid-July), a uniform mode is the dominant pattern of the southeastern China, which is related to preceding tropical signals and stronger WNP monsoon trough. Webster *et al.* (1998) proposed that this asymmetry could be explained by the seasonally varying east-west sea surface temperature (SST) gradients over the equatorial Pacific and Indian Oceans. In the Western Hemisphere, this precipitation asymmetry is related to the seasonal variations in the equatorial cold tongues in the Pacific and Atlantic (Wang and Ding, 2008) as well as the asymmetrical locations of the spring and fall intertropical convergence zones (ITCZs) (Lau and Chan, 1983; Meehl, 1987; Stanfied *et al.*, 2015).

The seasonal asymmetry of synoptic system activities could also lead to precipitation contrast between seasons, also known as monsoon precipitation. In tropical regions, the precipitation is influenced by tropical synoptic systems, such as subtropical high, trough that affects convection activities and temperature gradient (Feng and Fu, 2009; Feng *et al.*, 2009; Xu *et al.*, 2020). In addition, tropical and extratropical cyclones, leading to local circulation changes and heat flux or water vapor transportation, could affect local precipitation in a synoptic scale (Jiang and Zipser, 2010; Zhang *et al.*, 2020).

Studies of the second precipitation mode, *i.e.*, equinoctial asymmetric mode, have focused on the regional scale. However, although this mode also contributes to GM precipitation, a link between these precipitation regions and a complete explanation of its mechanisms remains to be elucidated. In addition, monsoons occur not only in tropical regions but also in certain mid- to high-latitude regions (Li and Zeng, 2000). Therefore, in this paper, we extend the GM domain from the tropics to the global region. Moreover, the precipitation formation is complex, since plenty of factors impact the tropical and midlatitude precipitations. This work aims to study the extended spring–autumn precipitation mode of the GM and determine its possible formation mechanisms.

This paper is organized as follows. Section 2 introduces the data which were used in this work. Section 3 presents the distribution and variations in the spring–autumn precipitation reversal pattern. Section 4 examines the possible formation mechanisms of GSAM. Finally, Section 5 provides the conclusion.

2 Data

The monthly precipitation dataset used is the Global Precipitation Climatology Project (GPCP) version 2.3 combined data from 1979 to present (Adler *et al.*, 2003), with a horizontal resolution of 2.5˚×2.5˚. The daily precipitation dataset used to calculate the long-term average of precipitation annual cycle is the GPCP daily dataset from 1996 to present. The monthly atmospheric field data (resolution 2.5˚×2.5˚), including sea level pressure (SLP), geopotential height, horizontal wind, and specific humidity, are obtained from the National Centers for Environmental Prediction (NCEP)/National Center for Atmospheric Research (NCAR) Reanalysis I dataset from 1948 to present (Kalnay, 1996). The monthly SST data are retrieved from Centennial *in situ* Observation-Based Estimates (COBE)-SST datasets from 1891 to present (Ishii *et al.*, 2005), with a resolution of 1˚×1˚. The tropical cyclone track datasets are obtained from the China Meteorological Administration (CMA) tropical cyclone best-track database from 1949 to present (Ying *et al.*, 2014). The analysis period considered for this study is from 1979 to 2017.

3 Distribution and Precipitation Variability of the GSAM Domain

3.1 Definition of the GSAM Domain

Fig.1 shows the two leading modes based on empirical orthogonal function (EOF) analysis of the global 12-month climatological precipitation. The first mode of EOF (Fig.1a) accounts for 64.7% of the total variance, which is a smaller contribution compared with the result of Wang and Ding (2008). The first mode exhibits an annual variation with a maximum in summer and minimum in winter (Fig.1a). The spatial pattern reveals a contrast between the Northern and Southern Hemispheres, in which asymmetric centers are located in tropical regions, with more precipitation during local summer and less precipitation during local winter in both hemispheres.

The second mode of EOF (Fig.1b) shows an annual cycle with a contrast between local autumn and spring. The spatial pattern reveals that most asymmetric precipitation centers mainly occur over oceans and partly on lands and could be divided into two parts by a division of 30˚N, which are the tropical region between 30˚S and 30˚N and the midlatitude region in 30˚N and its north. The midlatitude region features a wet autumn and a dry spring, while the distribution in the tropical region shows a more complex pattern. The second mode of EOF represents a positive-negative-positive triple pattern or a reversal pattern, with a contrast between tropical Indian Ocean–South China Sea and tropical Pacific–Atlantic. In tropical Indian Ocean–South China Sea area, the mode indicates a wet period from October to November and a dry period from April to May in equatorial regions and a dry period from October to November and a wet period from April to May off the equatorial regions of both hemispheres, which is due to asymmetric Asia summer monsoon onset-retreat dates and asymmetric circulations. Meanwhile, in the tropical Pacific and Atlantic area, the mode indicates a dry period from October to November and a wet period from April to May in equatorial regions and a wet period from October to November and a dry period from April to May off the equatorial regions of both southern and northern hemispheres, which is related to ITCZ location and tropical cold tongue in the Pacific and Atlantic.

The second mode accounts for 18% of the total variance, and its variance contribution is larger compared with the results of Wang and Ding. There are two possible explanations for this change: 1) the monsoon domain is extended from the tropical scale to the global scale, such that mid- and high-latitude precipitation contribute to the second mode, and 2) the frequency of the second mode in recent years has increased and has become more important than before. In this work, the second mode is defined as the global spring–autumn monsoon (GSAM).

Based on the EOF analysis results and the GM definition of Wang and Ding (2006), the GSAM domain is defined, and the following two conditions must be satisfied. First, as shown in Fig.2a, the precipitation difference between spring and autumn (October and November minus April and May or April and May minus October and November) exceeds 2 mm d^{-1}. Second, the precipitation rate of the wet season (the maximum of October and November or that of April and May) exceeds 20%, which means that the local precipitation in the wet season calculates 20% or more of total annual rainfall, as shown in Fig.2b. These two conditions are used to identify the regions with a more notable contrast and more precipitation during the wet season, respectively, compared with the global average of precipitation difference between spring and autumn which is 1.7 mm d^{-1} and global average precipitation rate in wet season which is about 18.2%. As a consequence, Fig.2c shows the GSAM domain, which is mainly distributed over oceans, partly located in the tropical Pacific and Atlantic, and the remainder is distributed over midlatitude oceans in the Northern Hemisphere.

3.2 GSAM Precipitation Index

In precipitation variation research, determining the precipitation intensity quantitatively is very important. In this work, the annual precipitation range between autumn and spring is used to measure the intensity of monsoon precipitation and is defined as the global spring – autumn monsoon index (SAI). A positive value indicates that the GSAM is strong in a particular year with more precipitation in local autumn and less precipitation in spring. Fig.3 shows the normalized SAI time series from 1979 to 2017, as well as the SAI in the Northern and Southern Hemispheres or in the tropical and midlatitude regions and the precipitation in local spring and in local autumn. As presented in Table 1, the correlation coefficients between the global SAI and the Northern Hemisphere SAI, tropical SAI, and local autumn precipitation are 0.91, 0.99, and 0.57, respectively, which all represent significance at the 95% confidence level. This indicates that the precipitation in the tropical domain of the Northern Hemisphere during local autumn dominates the variation in GSAM precipitation.

Among these 39 years, the strong GSAM years, *e.g.*, 1983, 1984, and 1998, correspond to decaying El Niño years, and the weak GSAM year, *e.g.*, 1997, corresponds to developing El Niño years, indicating a negative relationship between the GSAM precipitation and ENSO (El

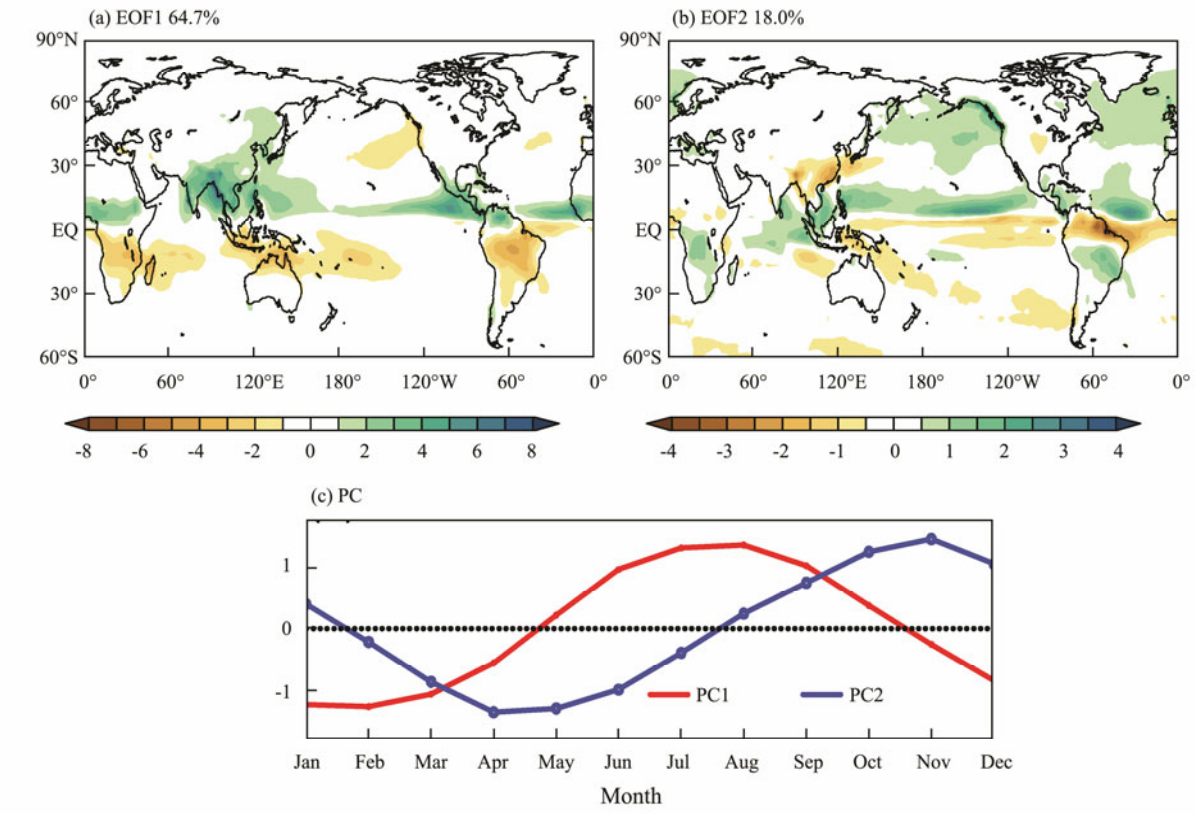

Fig.1 Spatial pattern of the long-term mean global precipitation (unit: mm d^{-1}): (a), the first mode; (b), the second mode; and (c) the corresponding principal components of the two modes.

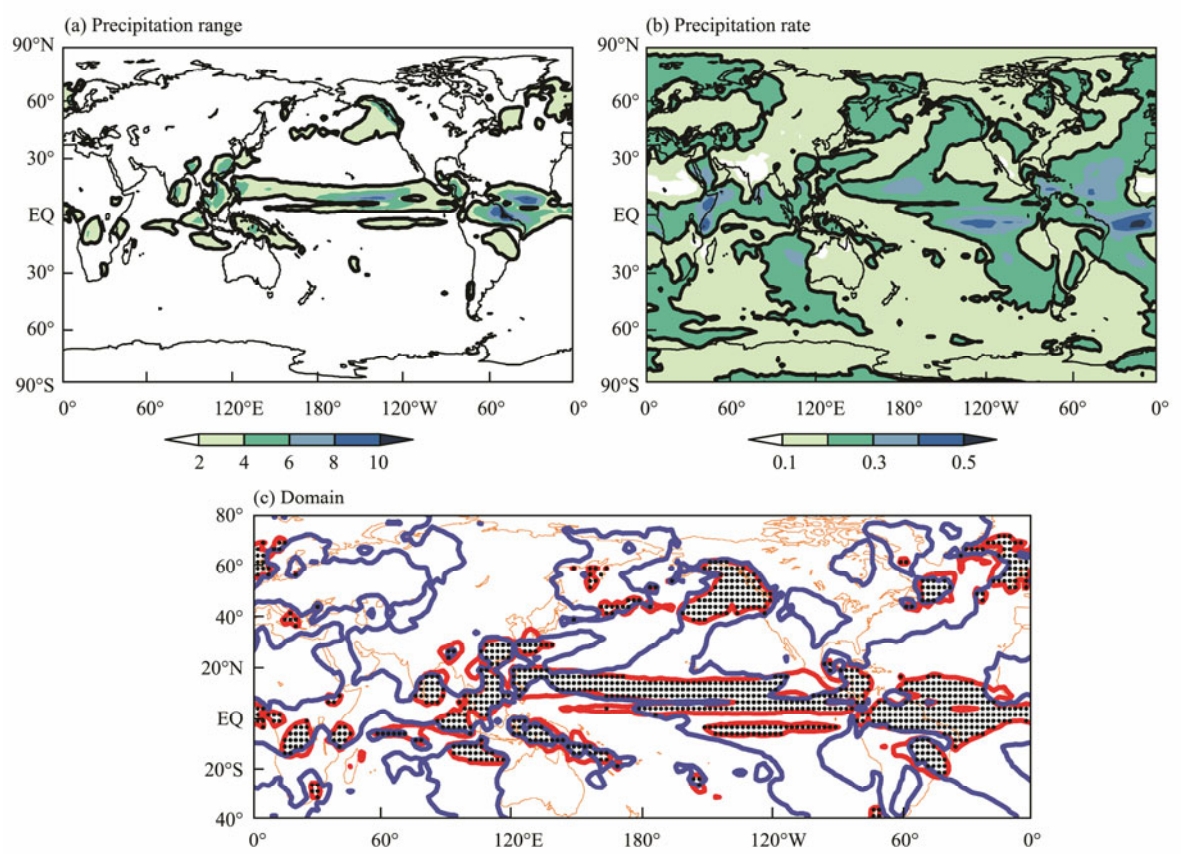

Fig.2 (a), Climatological mean of the annual precipitation range (unit: mm d^{-1}), the dashed lines indicate that the annual range exceeds 2 mm d^{-1}; (b), Climatological mean of the wet season precipitation rate, the dashed lines indicate that the precipitation rate exceeds 20%; (c), Definition of the global spring–autumn monsoon domain, the red lines indicate that the annual range exceeds 2 mm d^{-1}, and the blue lines indicate that the precipitation rate exceeds 20%, while the dotted regions indicate the global spring–autumn monsoon domain.

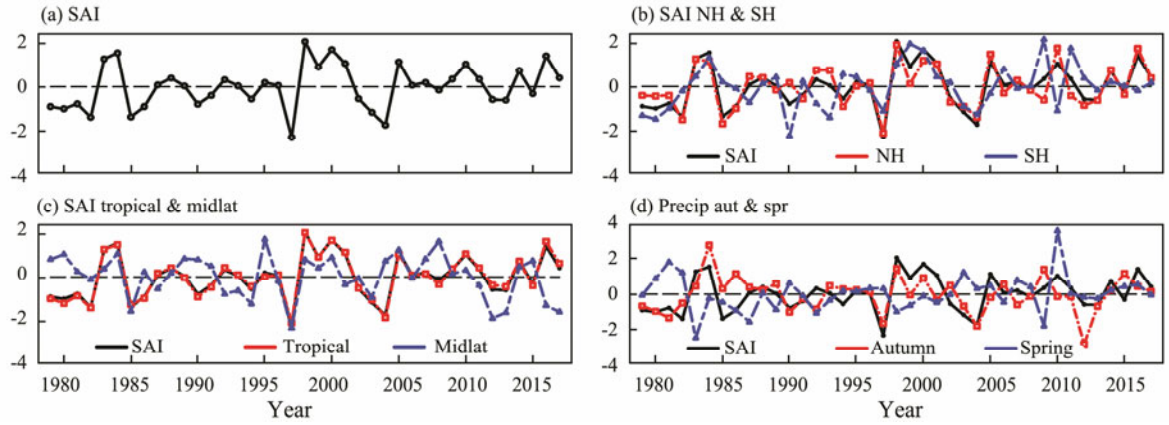

Fig.3 Time series of the normalized (a), global SAI; (b), SAI in the Northern and Southern Hemispheres; (c), SAI in the tropical and midlatitude regions; (d), precipitation in local spring and autumn (unit: mm d^{-1}).

Table 1 Correlation coefficient between global SAI and different parts of SAI

	Correlation coefficient
Northern Hemisphere	0.91
Southern Hemisphere	0.53
Tropical	0.99
Midlatitudes	0.31
Local autumn	0.57
Local spring	−0.22

Niño and Southern Oscillation) events. The correlation coefficient between the SAI and the Niño 3.4 index of December (0)–January–February (1) is −0.58, representing significance at the 95% confidence level. The positive GSAM years, *e.g.*, 1983, 1984, 1998, 1999, and 2000, are consistent with La Niña years or the decaying El Niño years, and the negative GSAM years, *e.g.*, 1982, 1990, 1997, 2004, and 2012, are consistent with the developing El Niño years.

4 Possible Formation Mechanisms of GSAM Precipitation

The formation mechanisms of GSAM precipitation are different in each domain due to its wide distribution. In this work, the GSAM domain is divided into three parts, namely, the tropical monsoon domain of the Eastern Hemisphere (northern Indian Ocean, South China Sea (SCS), and tropical WNP), the tropical monsoon domain of the Western Hemisphere (tropical eastern Pacific and Atlantic), and the midlatitude monsoon domain (the midlatitude Pacific and Atlantic of the Northern Hemisphere). Each part is analyzed separately.

4.1 Tropical Domain of the Eastern Hemisphere

The tropical GSAM domain of the Eastern Hemisphere is located in the tropical oceans around East Asia and South Asia, which is the largest classical winter–summer monsoon area named the Asia–Australia monsoon area. The tropical summer monsoon in the Indian Ocean, the South China Sea, and the Western Tropical Pacific is considerably asymmetrical regarding the times of onset and retreat (Wang *et al.*, 2004). The summer monsoon often breaks abruptly in late May, reaches the strongest period during July and August, and finally retreats slowly and transforms into the winter monsoon phase (Bombardi *et al.*, 2019). Thus, in the tropical GSAM domain of the Eastern Hemisphere, asymmetrical precipitation occurs between local spring and autumn due to the asymmetric onset and retreat of the summer monsoon regions including the whole tropical monsoon regions of 70°–150°E, 5°–20°N (Fig.4). In April and May, the winter monsoon affects the GSAM domain of the Northern Hemisphere, resulting in less precipitation, while the austral summer monsoon affects the GSAM domain of the Southern Hemisphere, resulting in more precipitation. In October and November, the boreal summer monsoon influences the GSAM domain of the Northern Hemisphere, resulting in more precipitation, while by the winter monsoon influences the GSAM domain of the Southern Hemisphere, resulting in less precipitation.

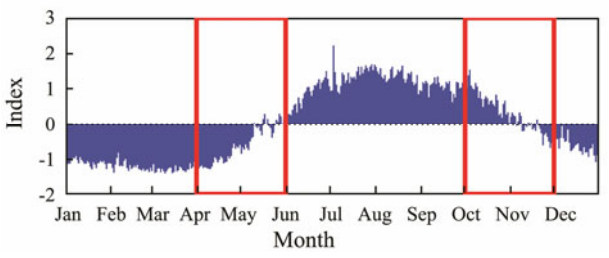

Fig.4 Climatological monsoon precipitation index of the tropical Asia summer–winter monsoon domain (70°–150°E, 5°–20°N). The red blocks indicate the periods of April to May and October to November (unit: mm d^{-1}).

Additionally, the SCS and WNP are the largest areas with tropical cyclone activities, with an average of about 30 tropical cyclones developing each year, accounting for more than one-third of the total quantity (Walsh *et al.*, 2016), and approximately 40% of the total precipitation is attributed to the tropical cyclonic activities over the SCS and WNP (Chen and Fu, 2015). As a result, the precipitation over the SCS and WNP is affected by tropical cyclone activities. Tropical cyclones are most active during local summer and autumn (Jiang and Zipser, 2010). In the SCS and WNP, the tropical cyclone frequency in October and November is higher than that in April and May (Fig.5). More tropical cyclone activities could result in more precipitation (Kubota and Wang, 2009; Jiang and Zipser, 2010). Therefore, the difference in tropical cyclone activities between local spring and autumn is one of the reasons for GSAM precipitation formation.

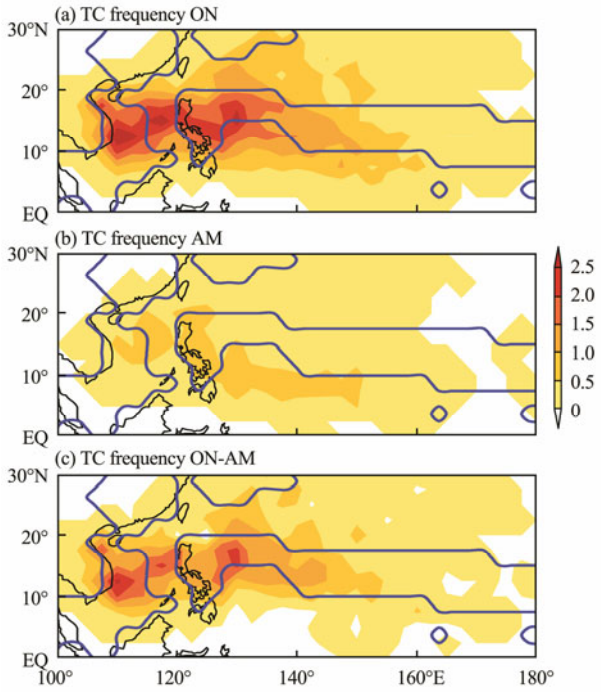

Fig.5 Climatological tropical cyclone frequencies over the western North Pacific and South China Sea (a) in October and November and (b) in April and May and (c) the differences between the two seasons. The blue lines indicate the spring–autumn monsoon domain.

4.2 Tropical Domain of the Western Hemisphere

The tropical GSAM domain of the Western Hemisphere includes the tropical eastern Pacific and tropical Atlantic, which are mainly affected by tropical cold tongues and ITCZ location. The intensity of the equatorial SST cold tongues in the eastern Pacific and eastern Atlantic, defined as SST average in 150°–80°W, 5°S–5°N, and in 20°W–0°, 5°S–5°N, respectively, exhibits notable annual variations (Fig.6), which are the lowest during the boreal spring and the highest during the boreal autumn (Okumura and Xie, 2004). These variations are a response of the coupled atmosphere-ocean system to solar forcing (Wang, 1994a). Therefore, GSAM precipitation is influenced by the intensity of the equatorial SST cold tongues, which has an impact on the ITCZ location. A strong cold tongue

indicates a cool equatorial SST, and the ITCZ forms off the equator in the Northern Hemisphere. A weak cold tongue indicates a warm equatorial SST, and the ITCZ moves southward near the equator or even south of the equator (Xie, 1994). The ITCZ represents deep convection activities and increasing precipitation. In October and November, the SST cold tongue is strong, and the ITCZ is located at approximately 10°N, resulting in more precipitation in the Northern Hemisphere GSAM domain and less precipitation in the Southern Hemisphere GSAM domain (Fig.7a). In April and May, the SST cold tongue is weak, and the ITCZ moves to the south of the equator, leading to increased precipitation in the Southern Hemisphere GSAM domain (Fig.7b).

At the same time, seasonal variations in the subtropical high also influence the monsoon precipitation. In April and May, the transitional seasons of the boreal winter to the summer, sunlight moves from the Southern Hemisphere to the Northern Hemisphere. During this period, the Northern Hemisphere gradually warms up, and the subtropical high intensifies. Moreover, the Southern Hemisphere cools down, and the subtropical high weakens (Fig.8b). An enhanced subtropical high affects the GSAM domain of the Northern Hemisphere, which means less and weaker convection activities (Mao *et al.*, 2003). As a result, compared with the Southern Hemisphere during April and May, there is less precipitation in the GSAM domain of the Northern Hemisphere. In October and November, the transitional seasons of the boreal summer to the winter, sunlight moves from the Northern Hemisphere to the Southern Hemisphere. The subtropical high strengthens in the Southern Hemisphere but weakens in the Northern Hemisphere (Fig.8a). An enhanced subtropical high affects the GSAM domain of the Southern Hemisphere, with less and weaker convection activities (Feng and Fu, 2009; Feng *et al.*, 2009; Li *et al.*, 2012). In conclusion, there is more precipitation during local autumn than during local spring in the GSAM domain of both hemispheres.

4.3 Midlatitude Domain in the Northern Hemisphere

In contrast to the tropical domain, GSAM precipitation in the midlatitude domain is mainly caused by the difference in water vapor transportation and convergence between local spring and autumn. In October and November, there is notable water vapor transportation through the midlatitudes of the Pacific and Atlantic as well as strong water vapor convergence (Fig.9a). In April and May, less notable water vapor transportation and convergence occur-

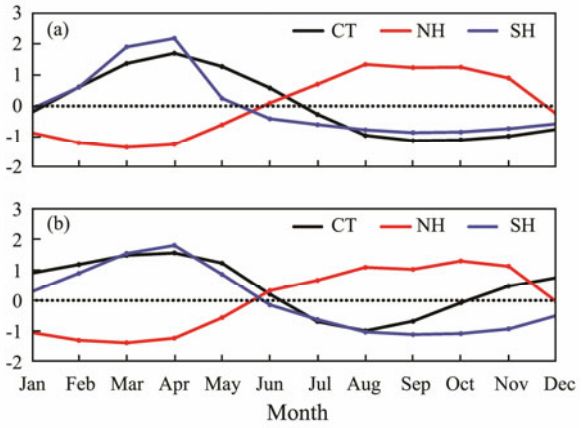

Fig.6 Annual variation in (a) the SST cold tongue (unit: ℃) and precipitation (unit: mm d^{-1}) over the eastern Pacific and (b) the SST cold tongue (unit: ℃) and precipitation (unit: mm d^{-1}) over the Atlantic.

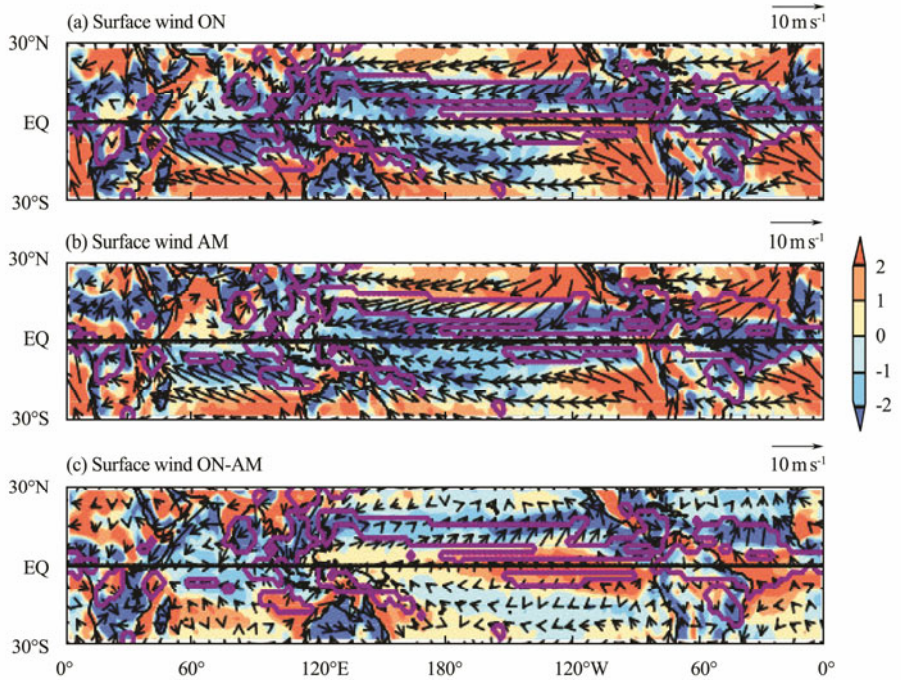

Fig.7 The same as in Fig.5 but for the climatological surface wind (vector) and convergence (shaded, unit: 10^{-6} s^{-1}).

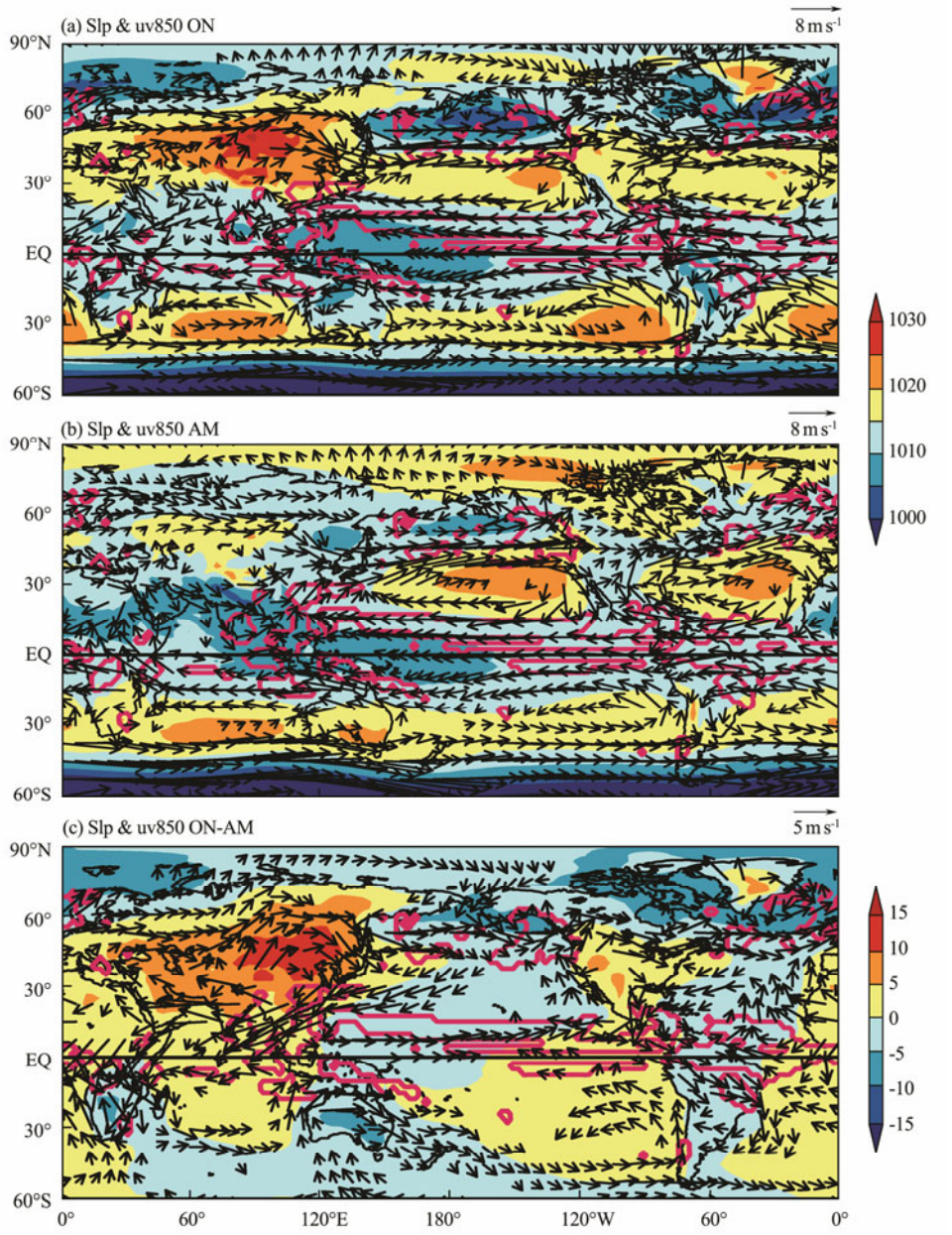

Fig.8 The same as in Fig.5 but for the climatological sea level pressure (shaded, unit: hPa) and wind at 850 hPa (vector).

through the GSAM domain (Fig.9b). Therefore, there is more precipitation in the GSAM domain during October and November than during April and May.

In addition, the midlatitude area is also influenced by extratropical cyclone activities, which are always controlled by the intensity and location of storm tracks, calculated using the Euler method based on the synoptic scale for 500 hPa geopotential height (Chang *et al.*, 2002). In addition, extratropical cyclonic activities could bring more precipitation by affecting oceanic and atmospheric circulation of the Northern Hemisphere (Rogers, 1997; Zhu *et al.*, 2001). Stronger storm tracks and more frequent extratropical cyclonic activities occur during October and November compared with April and May, and the Pacific storm tracks are shifted northward during October and November, bringing more precipitation to the GSAM domain (Fig.10). Thus, GSAM precipitation in the midlatitude domain is also influenced by extratropical cyclone activities.

5 Discussion and Conclusions

In this paper, the GM equinoctial asymmetric mode was defined as the GSAM, and the precipitation distribution was examined. The GSAM domain is mainly distributed over oceans: one part is located in the midlatitudes of the Pacific and Atlantic, while the other part is asymmetrically located over the tropical ocean. In the GSAM domains of both hemispheres, more precipitation occurs in local autumn than in local spring. The spatial distributions of precipitation and GSAM domain are mainly induced by the large-scale atmospheric circulations.

In the tropical domain of the Eastern Hemisphere, GSAM precipitation is mainly influenced by two factors, namely, the onset and retreat of the classical winter–summer monsoon and the tropical cyclone activities over

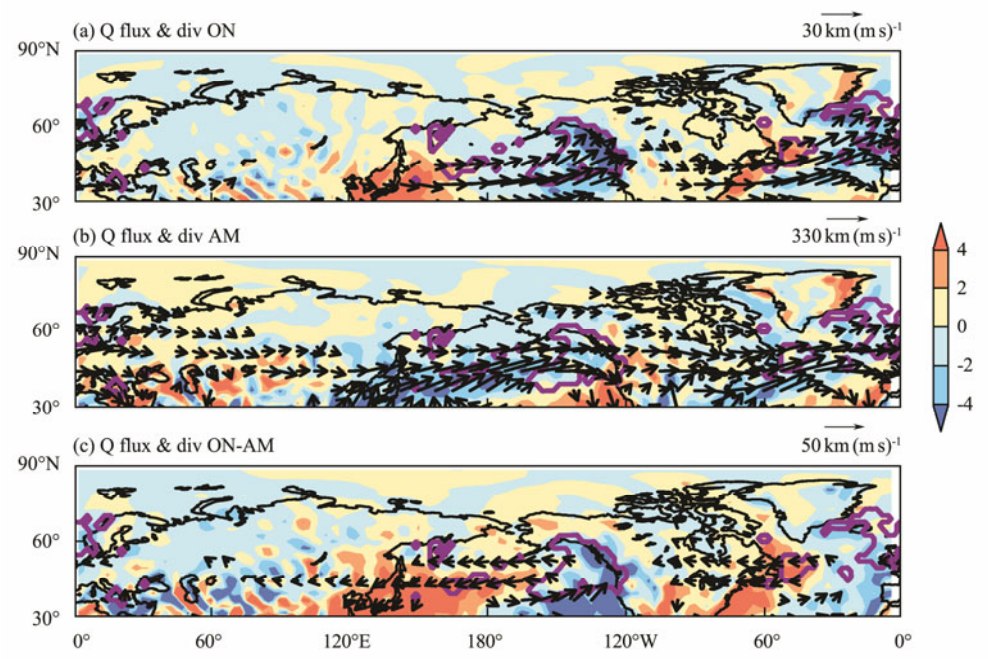

Fig.9 The same as in Fig.5 but for the climatological integrated water vapor flux (vector) and convergence (shaded, unit: $0.01\,\mathrm{kg\,(m^2\,s)^{-1}}$).

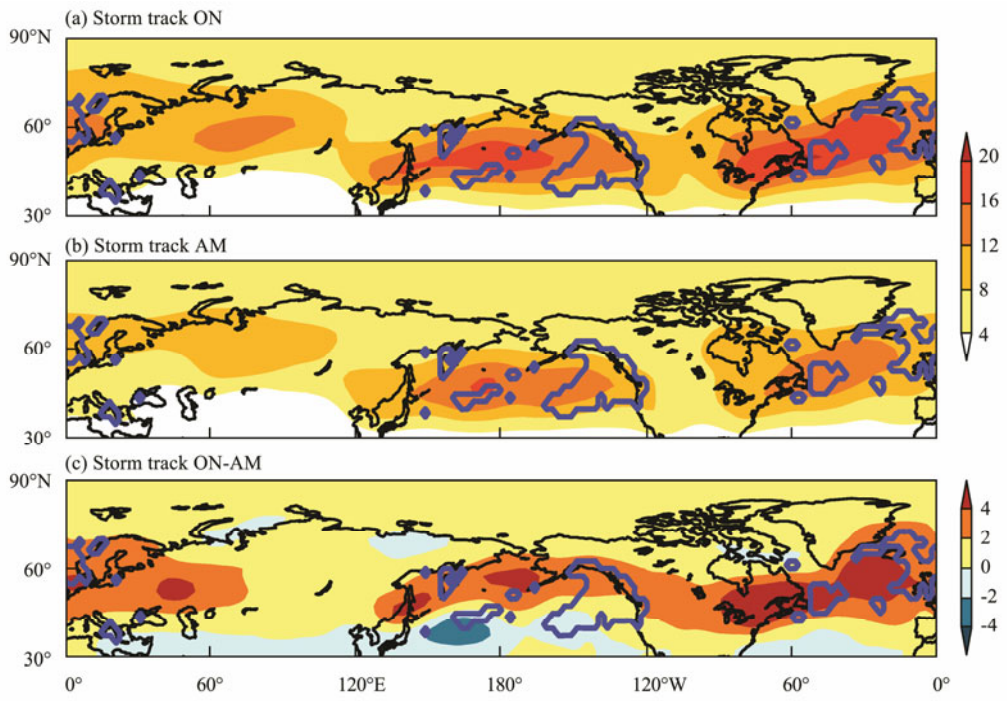

Fig.10 The same as in Fig.5 but for the climatological storm tracks (unit: $\mathrm{dagpm^2}$).

the SCS and WNP, which could bring more precipitation to the GSAM domain in boreal autumn.

In the tropical domain of the Western Hemisphere, GSAM precipitation is mainly influenced by the tropical asymmetrical circulation in the Northern and Southern Hemispheres, with a stronger subtropical high in local spring and a weaker subtropical high in local autumn. Additionally, the SST cold tongues over the equatorial eastern Pacific and eastern Atlantic have an impact on the ITCZ, and the deep convection in the ITCZ area could provide more precipitation to the GSAM domain.

In the midlatitude domain, GSAM precipitation is caused by the seasonal differences in water vapor transportation and convergence over the GSAM domain, which is stronger in the boreal autumn than in spring. In addition, GSAM precipitation is also influenced by extratropical cyclone activities. There are more and stronger extratropical cyclone activities during the boreal autumn, bringing more precipitation to the GSAM domain.

In this work, we consider the differences between the spring and autumn atmospheric circulation as the causes of GSAM. However, these circulations directly affecting

the asymmetric precipitation pattern may not be the most fundamental causes of GSAM precipitation. As shown in Fig.1b, there are wet lands and dry oceans during local spring and dry lands and wet oceans during local autumn in both the Southern and Northern Hemispheres in the EOF2 mode. This implies that the GSAM also shows a feature of ocean-land contrast. It can be regarded as a delayed response to solar forcing due to atmosphere-ocean-land interaction and thermal inertia. The land-ocean heat capacity could lead to asymmetric warming up of land and ocean regions, thus regulating the land-ocean thermal contrast and even different circulations. On the other hand, in tropical cold tongue regions, the atmosphere-ocean interaction determines the delayed oceanic response to solar forcing. Wang (1994b) pointed out that the tropical eastern Pacific exhibits two annual cycle modes. The first one is a monsoon mode directly driven by solar forcing, while the other one is a coupled equatorial-coastal mode which originated from atmosphere-ocean interaction, corresponding to the annual cycle of cold tongue intensity and related ITCZ, leading to an asymmetric precipitation pattern during transition seasons. The essential reasons for the GSAM needs further careful study. In addition, the interannual and interdecadal variations in GSAM precipitation still need more investigations.

Acknowledgements

The work was supported by the Global Change Research Program of China (No. 2019YFA0607004) and the National Natural Science Foundation of China (Nos. 41575067, 41975061).

References

Adler, R. F., Huffman, G. J., Chang, A., Ferraro, R., Xie, P., Janowiak, J., *et al.*, 2003. The Version 2 Global Precipitation Climatology Project (GPCP) monthly precipitation analysis (1979-present). *Journal of Hydrometeorology*, **4**: 1147-1167.

Bombardi, R. J., Moron, V., and Goodnight, J. S., 2019. Detection, variability, and predictability of monsoon onset and withdrawal dates: A review. *International Journal of Climatology*, **40** (2): 641-667.

Chang, C. P., Wang, Z., McBride, J., and Liu, C. H., 2005. Annual cycle of Southeast Asia-Maritime continent rainfall and the asymmetric monsoon transition. *Journal of Climate*, **18**: 287-301.

Chang, E. K. M., Lee, S., and Swanson, K. L., 2002. Storm track dynamics. *Journal of Climate*, **15**: 2163-2183.

Chao, W. C., 2000. Multiple quasi equilibria of the ITCZ and the origin of monsoon onset. *Journal of the Atmospheric Sciences*, **57** (57): 641-652.

Chen, F. J., and Fu, Y. F., 2015. Contribution of tropical cyclone rainfall at categories to total precipitation over the western North Pacific from 1998 to 2007. *Science China Earth Sciences*, **58** (11): 2015-2025.

Feng, S, and Fu, Y. F., 2009. Seasonal characteristics of precipitation occurrences in the core area of the subtropical high. *Acta Meteorologica Sinica*, **23**: 681-690.

Feng, S., Qi, L., and Fu, Y. F., 2009. Precipitation under subtropical high conditions: Evidence and implications. *Atmospheric and Oceanic Science Letters*, **2** (4): 60-65.

Gadgil, S., 2003. The Indian monsoon and its variability. *Annual Review of Earth and Planetary Sciences*, **22** (4): 29-67.

Ishii, M., Shouji, A., Sugimoto, S., and Matsumoto, T., 2005. Objective analyses of sea-surface temperature and marine meteorological variables for the 20th century using ICOADS and the kobe collection. *International Journal of Climatology*, **25**: 865-879.

Jiang, H., and Zipser, E. J., 2010. Contribution of tropical cyclones to the global precipitation from eight seasons of TRMM data: Regional, seasonal, and interannual variations. *Journal of Climate*, **23** (6): 1526-1543.

Kalnay, E., 1996. NCEP/NCAR 40-year reanalysis project. *Bulletin of the American Meteorological Society*, **77** (3): 437-472.

Kim, H. J., Wang, B., and Ding, Q. H., 2008. The global monsoon variability simulated by CMIP3 coupled climate models. *Journal of Climate*, **21** (20): 5271-5294.

Kubota, H., and Wang, B., 2009. How much do tropical cyclones affect seasonal and interannual rainfall variability over the western North Pacific? *Journal of Climate*, **22** (20): 5495-5510.

Lau, K. M., and Chan, P. H., 1983. Short-term climate variability and atmospheric teleconnections from satellite-observed outgoing long wave radiation. Part II: Lagged correlations. *Journal of Aerosol Science*, **40**: 2751-2767.

Li, J. P., and Zeng, Q. C., 2000. Significance of the normalized seasonality of wind field and its rationality for characterizing the monsoon. *Science in China Series D: Earth Sciences*, **43**: 646-653, DOI: 10.1007/BF02879509.

Li, L., Li, W., and Kushnir, Y., 2012. Variation of the North Atlantic subtropical high western ridge and its implication to southeastern US summer precipitation. *Climate Dynamics*, **39** (6): 1401-1412.

Liu, F., Ouyang, Y., Wang, B., Yang, J., and Hsu, P. C., 2020. Seasonal evolution of the intraseasonal variability of China summer precipitation. *Climate Dynamics*, **54**: 4641-4655, https://doi.org/10.1007/s00382-020-05251-0.

Liu, J., Kuang, X. Y., Wang, B., Ding, Q. H., Soon, W., and Zorita, E., 2009. Centennial variations of the global monsoon precipitation in the last millennium: Results from ECHO-G model. *Journal of Climate*, **22** (9): 2356-2371.

Mao, J. Y., Wu, G. X., and Liu, Y. Q., 2003. Study on the variation in the configuration of subtropical anticyclone and its mechanism during seasonal transition–Part I: Climatological features of subtropical high structure. *Acta Meteorologica Sinica*, **17** (3): 274-286.

Meehl, G. A., 1987. The annual cycle and interannual variability in the tropical Pacific and Indian Ocean regions. *Monthly Weather Review*, **115**: 27-50.

Okumura, Y., and Xie, S. P., 2004. Interaction of the Atlantic equatorial cold tongue and the African monsoon. *Journal of Climate*, **17** (18): 3589-3602.

Rogers, J. C., 1997. North Atlantic storm track variability and its association to the North Atlantic oscillation and climate variability of northern Europe. *Journal of Climate*, **10** (7): 1635-1647.

Stanfield, R., Dong, X., Xi, B., Su, H., Donner, L., Rotstayn, L., *et al.*, 2015. A quantitative assessment of precipitation associated with the ITCZ in the CMIP5 GCM simulations. *Climate Dynamics*, **47**: 1863-1880, DOI: 10.1007/s00382-015-2937-y.

Walsh, K. J. E., Mcbride, J. L., Klotzbach, P. J., Balachandran, S., Camargo, S. J., and Holland, G., 2016. Tropical cyclones and climate change. *Wiley Interdisciplinary Reviews: Climate Change*, **7** (1): 65-89.

Wang, B., 1994a. Climatic regimes of tropical convection and rainfall. *Journal of Climate*, **7**: 1109-1118.

Wang, B., 1994b. On the annual cycle in the tropical eastern central Pacific. *Journal of Climate*, **7**: 1926-1942, https://doi.org/10.1175/1520-0442(1994)007<1926:OTACIT>2.0.CO;2.

Wang, B., and Ding, Q., 2006. Changes in global monsoon precipitation over the past 56 years. *Geophysical Research Letters*, **33**: L06711, DOI: 10.1029/2005GL025347.

Wang, B., and Ding, Q., 2008. Global monsoon: Dominant mode of annual variation in the tropics. *Dynamics of Atmospheres and Oceans*, **44** (2-3): 165-183, DOI: 10.1016/j.dynatmoce.2007.05.002.

Wang, B., Kim, H. J., Kikuchi, K., and Kitoh, A., 2011. Diagnostic metrics for evaluation of annual and diurnal cycles. *Climate Dynamics*, **37** (5-6): 941-955.

Wang, B., LinHo, Zhang, Y., and Lu, M. M., 2004. Definition of South China Sea monsoon onset and commencement of the East Asia summer monsoon. *Journal of Climate*, **17** (4): 699-710.

Wang, B., Liu, J., Kim, H. J., Webster, P. J., and Yim, S. Y., 2012. Recent change of the global monsoon precipitation (1979–2008). *Climate Dynamics*, **39** (5): 1123-1135.

Webster, P. J., Magana, V. O., Palmer, T. N., Shukla, J., Tomas, R. A., Yanai, M., *et al.*, 1998. Monsoons: Processes, predictability, and the prospects for prediction. *Geophysical Research Letters* **103**: 14451-14510.

Xie, S. P., 1994. The maintenance of an equatorially asymmetric state in a hybrid coupled GCM. *Journal of the Atmospheric Sciences*, **51** (18): 2602-2612.

Xu, H., Goldsmith, Y., Lan, J., Tan, L., Wang, X., and Zhou, X., 2020. Juxtaposition of western Pacific subtropical high on Asian summer monsoon shapes subtropical East Asian precipitation. *Geophysical Research Letters*, **47**: e2019GL084705, https://doi.org/10.1029/2019GL084705.

Ying, M., Zhang, W., Yu, H., Lu, X., Feng, J., Fan, Y., *et al.*, 2014. An overview of the China Meteorological Administration tropical cyclone database. *Journal of Atmospheric and Oceanic Technology*, **31**: 287-301, DOI: 10.1175/JTECH-D-12-00119.1.

Zhang, A., Chen, Y., Zhang, Q., Zhang, X., and Fu, Y., 2020. Structure of cyclonic precipitation in the northern Pacific storm track measured by GPM DPR. *Journal of Hydrometeorology*, **21** (2): 227-240, DOI: 10.1175/JHM-D-19-0161.1.

Zhou, T., Yu, R., Li, H., and Wang, B., 2008. Ocean forcing to changes in global monsoon precipitation over the recent half-century. *Journal of Climate*, **21** (15): 3833-3852.

Zhu, W. J., Sun, Z. B., and Zhou, B., 2001. The impact of pacific SSTA on the interannual variability of northern Pacific storm track during winter. *Advances in Atmospheric Sciences*, **18** (5): 1029-1042.

(Edited by Xie Jun)